

Deep Learning the Shape of the Brain Connectome

Haocheng Dai^{1,2}, Martin Bauer⁴, P. Thomas Fletcher⁵, and Sarang C. Joshi^{1,3}

¹ Scientific Computing and Imaging Institute, University of Utah
hdai@sci.utah.edu

² School of Computing, University of Utah

³ Department of Bioengineering, University of Utah

⁴ Department of Mathematics, Florida State University

⁵ Electrical and Computer Engineering, University of Virginia

Abstract. To statistically study the variability and differences between normal and abnormal brain connectomes, a mathematical model of the neural connections is required. In this paper, we represent the brain connectome as a Riemannian manifold, which allows us to model neural connections as geodesics. We show for the first time how one can leverage deep neural networks to estimate a Riemannian metric of the brain that can accommodate fiber crossings and is a natural modeling tool to infer the shape of the brain from DWMRI. Our method achieves excellent performance in geodesic-white-matter-pathway alignment and tackles the long-standing issue in previous methods: the inability to recover the crossing fibers with high fidelity.

Keywords: Deep learning · Diffusion weighted imaging · Riemannian geometry.

1 Introduction

Diffusion-weighted magnetic resonance imaging (DWMRI) enables the non-invasive study of neural connections within the living human brain. DWMRI measures the local diffusion of water within axonal bundles, allowing for local directional estimation of neural connections. Long distance structural connectivity of the brain is inferred by the process of tractography, which estimates white matter tracts via various streamlining algorithms. Deterministic tractography [1] computes the integral curves over the vector field associating the most likely direction of fiber tracts with each voxel. However, the simplest deterministic streamline tractography is sensitive to imaging noise and also easily confounded in the crossing-fiber region. Various approaches such as Kalman filtering [4,17], probabilistic tractography [2] and front propagation [8] have also been proposed. The collection of tracts in an individual brain estimated by one or the other

* M. Bauer was supported by NSF grants DMS-1912037, DMS-1953244. H. Dai, S. Joshi and P. Fletcher were supported by NSF grant DMS-1912030.

methods is referred to as the connectome.

Mathematical models for the shape of the connectome: To study the variability in normal populations and to find differences between neural connections in normal and abnormal brains, we need a precise mathematical model of the connectome. Traditionally, individual fiber tracts have been modeled as smooth curves without any intimate link to the underlying geometry of the brain. In this paper, we model the brain as a compact Riemannian manifold. A Riemannian manifold is a real, differentiable manifold M , equipped with a positive-definite inner product on the tangent space at each point. The shape of the Riemannian manifold is captured by the local metric. Smooth Riemannian manifolds with the same topology can have very different shapes because of the differing local metric structure. For example, spheres and ellipsoids have identical differential and topological structures, while the local Riemannian metric is different. In this paper, we assume that the topology of the anatomy of the normal human brain is consistent across individuals, yet the shape varies due to the differences in its local metric.

Related work: DWMRI is the foundation to model an individual brain as a Riemannian manifold. With the Riemannian-metric-equipped manifold, we can infer the white matter pathways and also the shape of an individual’s connectome. O’Donnell et al. [19] first proposed the geodesic tractography algorithm that uses the inverse of the diffusion tensor as the Riemannian metric and treats geodesic curves under the metric as white matter pathways. However, there is a tendency in the inverted-tensor metrics that the geodesic under it would easily deviate from the principal eigenvector direction in the high-curvature area. To address this issue, Fletcher et al. [8] enhanced the metric by “sharpening” the inverted-tensor metric, i.e., taking the eigenvalues of metric tensor to some power so as to increase the anisotropy. But this strategy does not take into account the spatially varying curvature of the vector field, and it increases the sensitivity to the noise. Fuster et al. [9] demonstrated that using the adjugate of the diffusion tensor field as the Riemannian metric gave improved geodesic tractography over the inverted sharpened metric while being more robust to imaging noise. In order to strengthen the adherence of geodesics to the white matter pathways, Hao et al. [12] developed an adaptive Riemannian metric by applying a conformal scalar field to the inverse of the diffusion tensor, which necessitates solving a Poisson equation on the Riemannian manifold. Campbell et al. [3] further advanced the Riemannian formulation of structural connectomes by introducing methods for diffeomorphic image registration and atlas building using the Ebin metric on the space of Riemannian metrics. These geodesic approaches have several advantages over traditional tractography, including improved robustness to imaging noise and the ability to find tracts between two given anatomical endpoints in cases where traditional tractography fails. However, their ability to characterize crossing fibers and align tractography with data is severely limited, as they are all derived from the diffusion tensor model. More modern modeling techniques, such as HARDI [23], Q-Ball [22] and DSI [24], are able to infer multiple fiber directions at each point in the brain.

Contributions: In this paper, we show for the first time how one can leverage the power of deep neural networks (DNNs) to estimate a metric structure of the brain that can accommodate fiber crossings and is a natural modeling tool to infer the shape of the brain from DWMRI. We formulate the metric estimation problem as a solution to a nonlinear system of partial differential equations (PDEs). DNNs have emerged as a promising tool to solve PDEs, see, e.g., [20]. In this work, we adopt convolutional encoder-decoder neural networks for estimating the Riemannian metric of human brains in a self-supervised manner. By using spatially discretized vector fields from any of the plethora of models for local fiber directions and a flexible network architecture, our method achieves excellent performance in terms of geodesic-white-matter-pathway alignment. In addition to simple deployment and boundary insensitivity, our approach also tackles the long-standing issue in previous methods: the inability to recover the crossing fibers with high fidelity. This paper is a novel algorithmic development paper, and as such, extensive validation of the inferred metric is beyond its scope. We show that the metric estimation is able to faithfully represent multiple vector fields as geodesic vector fields of the estimated metric. We inherit the validity of the tracts from the choice of the preferred local directional estimation algorithm, which is explicitly not the focus of this work.

2 Estimating Riemannian Metrics from Geodesics

In this section, we will introduce the inverse problem that will be at the center of our approach: the estimation of a Riemannian metric based on the observation of fiber directions as the tangents to geodesic curves. We will first recall some definitions and concepts from Riemannian geometry. For further details, we refer to classic textbooks such as [5,16]. In all of this work, our modeling space is a finite-dimensional manifold M (possibly with boundary). In our application, the topology of the manifold M will be rather trivial and thus we assume in the following that M is a bounded subset of \mathbb{R}^n with $n \in \{2, 3\}$. Next we introduce the concept of an integral curve: given a vector field $\mathbf{v} \in \mathfrak{X}(M)$, i.e., a map from M to TM , we call a curve $\gamma : \mathbb{R} \rightarrow M$ an integral curve of \mathbf{v} if $\gamma'(t) = \mathbf{v}(\gamma(t))$, i.e., the curve follows the flow lines of the vector field. A Riemannian metric g on M is a family of inner products on each tangent space $T_x M$ that depend smoothly on the base point, $x \in M$. Note that in local coordinates we can identify the Riemannian metric with a field of positive-definite, symmetric matrices $g(x)$, and the inner product between two tangent vectors $\mathbf{v}, \mathbf{w} \in T_x M$ is simply given by $\mathbf{v}^T g(x) \mathbf{w}$. We call a curve between p and q a (minimizing) geodesic if it minimizes the energy functional $E(\gamma) = \frac{1}{2} \int_0^1 g_\gamma(\partial_t \gamma, \partial_t \gamma) dt$. Locally length-minimizing curves satisfy an ordinary differential equation, called the geodesic equation, which is the first-order optimality condition $dE(\gamma) = 0$.

For every Riemannian manifold there exists a unique connection ∇^g , called the Levi-Civita covariant derivative, that encodes this notion of geodesic curves.

Given vector fields \mathbf{v} and \mathbf{w} , we can write a coordinate expression of ∇^g via

$$\nabla_{\mathbf{v}}^g \mathbf{w} = \sum_k \left(\sum_i v^i \frac{\partial w^k}{\partial x^i} + \sum_{i,j} \Gamma_{ij}^k v^i w^j \right) \mathbf{e}_k, \quad (1)$$

where $\mathbf{v} = \sum v^i \mathbf{e}_i$, $\mathbf{w} = \sum w^i \mathbf{e}_i$ with $\mathbf{e}_i = \frac{\partial}{\partial x^i}$ being the i -th basis vector. Furthermore, Γ_{ij}^k are the Christoffel symbols, which are defined as

$$\Gamma_{ij}^k = \frac{1}{2} \sum_{l=1}^n g^{kl} \left(\frac{\partial g_{jl}}{\partial x^i} + \frac{\partial g_{il}}{\partial x^j} - \frac{\partial g_{ij}}{\partial x^l} \right), \quad (2)$$

where g_{ij} denotes the entries of the Riemannian metric g , and g^{ij} represents the entries of the inverse of metric g^{-1} . Using this notation, the geodesic equation can be written as $\nabla_{\partial_t \gamma}^g \partial_t \gamma = 0$. Finally, we call a vector field a geodesic (vector) field if all its integral curves are geodesics, i.e., \mathbf{v} is a geodesic field if $\nabla_{\mathbf{v}}^g \mathbf{v} = 0$.

We are now able to formulate the inverse problem studied in this paper as:

Unregularized, exact metric estimation: Given vector fields $\mathbf{v}_i \in \mathfrak{X}(M)$, $i \in \{1, \dots, m\}$, find a Riemannian metric g on M such that all \mathbf{v}_i are geodesic vector fields, i.e., find a Riemannian metric such that $\nabla_{\mathbf{v}_i}^g \mathbf{v}_i = 0$ for all $i \in \{1, \dots, m\}$.

Using Eq. (1) to express the condition $\nabla_{\mathbf{v}_i}^g \mathbf{v}_i = 0$, this can be interpreted as a system of non-linear PDEs for the metric g . The inverse problem is in general highly ill-posed — there might exist either many solutions or no solution at all. Even in the case of a single vector field \mathbf{v} , the situation is far from being trivial, see e.g. [11] for characterization in the case of M being a surface, and [15] for examples where no solution exists. To deal with these difficulties, we consider instead the following variation of the above metric estimation problem:

Regularized, inexact metric estimation: Given vector fields $\mathbf{v}_i \in \mathfrak{X}(M)$, $i \in \{1, \dots, m\}$, find the Riemannian metric g on M that minimizes the energy functional

$$\mathcal{E}(g) = \sum_{i=1}^m \|\nabla_{\mathbf{v}_i}^g \mathbf{v}_i\|_{L^2} + \alpha \text{Reg}(g), \quad (3)$$

where $\alpha > 0$ is a weight parameter.

Here the first term enforces the condition that the vector fields \mathbf{v}_i are close to geodesic, while the second term is a regularization parameter that is responsible for the solution selection. We note that this formulation relates directly to the

physics-informed neural network formulation for solving PDEs using neural networks as described next. Furthermore, we will not add an explicit regularization term for the metric g . Instead, we will implicitly regularize our problem via our solution parameterization via a neural network.

3 Metric Estimation via Neural Networks

We now present a novel deep learning framework for solving the inverse problem formulated above. Physics-informed neural networks (PINNs), proposed by Raissi et al. [20], leverage the universal approximation ability of DNNs to estimate the solution of a PDE by encoding the inverse problem into the loss function. The automatic differentiation module embedded in most machine learning frameworks, such as `PyTorch` and `TensorFlow`, automates the process of finding the solution efficiently and mesh-freely. In our situation, this corresponds to the network representing a metric field, i.e., the input of the network is the coordinate $x \in \mathbb{R}^n$ and the output of the network is a symmetric matrix $s \in \mathbb{R}^{n \times n}$ at position x . To enforce the metric to be positive-definite, we use the matrix exponential operation to produce our final metric estimate, $g = \exp(s)$. As Eq. (2) can be evaluated exactly by the automatic differentiation module, we can efficiently evaluate our loss function. We want to repeat that we have not explicitly added a regularization term, but instead we rely on the implicit regularization properties of the network representation. In our experiments, the predictive ability and accuracy of PINNs decayed drastically as the dimension and complexity of the solution increased, and in particular, the performance of this solution representation did not scale up to the complex geometry of the human brain. To overcome the inherent limitation of the vanilla PINNs, we followed the method proposed by Zhu et al. [26], who employ a convolutional encoder-decoder neural network (CEDNN) approach to construct the multi-scale features from high-dimensional input. By incorporating the input, output fields, and corresponding differentiation field into the loss function, the network is trained to capture the heterogeneous mapping between the given fields and the resulting solution field. Thus, unlike the PINN architecture, CEDNN takes the whole spatially discretized vector fields as the input and outputs the entire metric field which minimizes Eq. (3). DenseNet [14] is a promising network architecture for this task. DenseNet furthers the ideas of residual learning in ResNet [13] and bypassing paths in highway networks [21] by concatenating every previous layer’s output as the input of the current layer in a feed-forward fashion. The dense connectivity improves the information flow in the network, without introducing any optimization difficulty. The encoder contracts the higher-level context and feature of the input, while the decoder commits to recovering the location information to the same scale as the original input fields. Our network takes an $m \times n$ -channel input, where n is the dimension of the vector fields and m is the number of distinct geodesic vector fields \mathbf{v}_i used for the metric estimation. By sending the concatenated vector fields into the network, CEDNN yields an output of $(n+1)n/2$ channels which infers the $(n+1)n/2$ distinct entries of an $n \times n$

symmetric matrix. We then form the final estimated metric, the $n \times n$ symmetric positive-definite matrix, also through the matrix exponential operation. As the spatial variable x is no longer explicit in the network, to compute spatial gradients, we adopt a central finite-difference scheme to approximate the derivatives in the loss function as given in Eq. (3). For more details on the architecture, see Fig. 1.

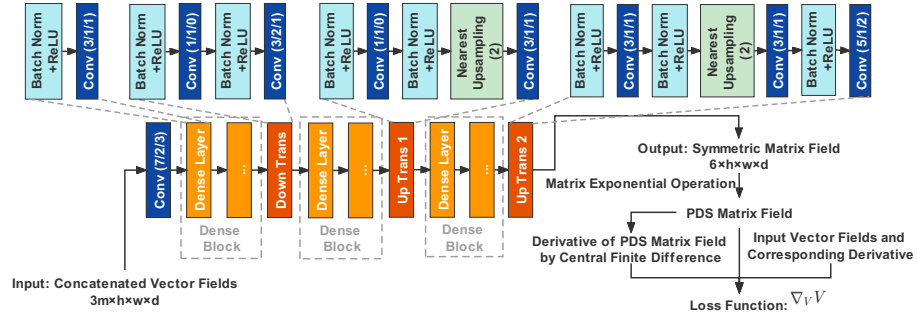


Fig. 1: The architecture of the proposed convolutional encoder-decoder neural networks. Here, h, w, d denote the shape of the input vector fields, and m represents the number of total vector fields. The numbers in a Conv box stand for the kernel size, stride, and padding of the convolution, respectively. The number in a Nearest Upsampling box indicates the scaling factor.

4 Experiments

In all the experiments presented below, we used a CEDNN to represent the metric, where we employed the **Adadelta** optimizer to minimize our loss function. All computations were carried out on a **Nvidia Titan RTX GPU**. The runtime for all experiments was approximately 4 seconds per iteration.

2D Brain Slice: For easy visualization and interpretability, we first compare our method with other geodesic tractography approaches on a projected 2D brain slice from the Human Connectome Project (HCP) [10] (subject 103818). Fig. 2 shows the geodesics w.r.t. the inverted diffusion tensor metric [19], the adjugate of the diffusion tensor [9], the conformal metric [12], and the metric estimated by our method. We quantitatively measured the geodesic-white-matter-pathway alignment of these methods by integrating geodesics from 30 randomly chosen seed points in the corpus callosum and calculating the mean error of the geodesic as compared to the integral curve of the vector field corresponding to the same seed point. The central panel in Fig. 2 shows one example of a geodesic, where one can clearly see that the geodesics of the other three methods deviate from the integral curve eventually, while ours proves a much better alignment to the ground truth. In the right panel, this observation is quantified: one can see that

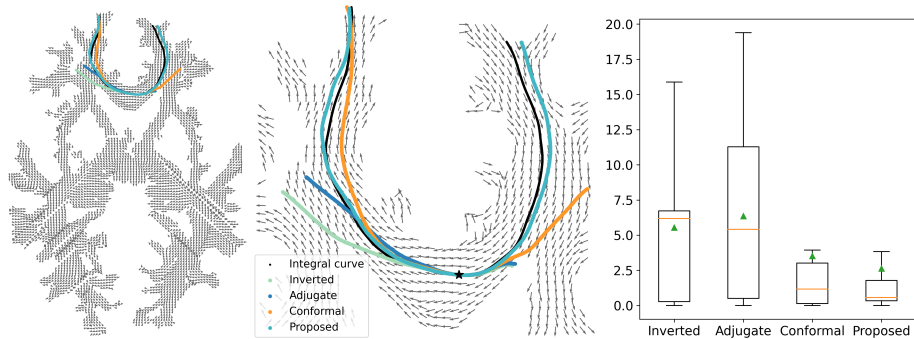


Fig. 2: Left: axial view of an HCP brain image. Central: detailed view of the geodesics and integral curve starting from the star. Right: Box plot of distances between the integral curve and geodesics generated by different methods. Green triangles stand for the mean values, and orange bars represent the median values.

our method outperforms the others in terms of both mean and median of mean errors.

2D Synthetic “Braid”: To verify and exemplify our method’s crossing fiber estimation ability, we synthesized two vector fields (see the first two panels in Fig. 3). The central integral curves of the vector bundle are two trigonometric functions: $x_2 = 20 \cos(\frac{1}{4\pi}(x_1 - 60)) + 50$ and $x_2 = 20 \sin(\frac{1}{4\pi}x_1) + 50$, where x_1, x_2 stand for pixel coordinates. The vector along the curve aligns with the corresponding tangent vector of the curve. We then constructed the vector bundle by parallel translating the central integral curve within nine pixels horizontally. For the solution, we used a CEDNN the following parameters: the number of dense layers in the three dense blocks are 6, 8, 6, with a growth rate of 16, where we used a learning rate of 0.0001 for the optimization. Fig. 3 shows the metric fields g (second panel from right) estimated by our method and the alignment of ground truth integral curves (black) and geodesics (indigo). In addition to the good alignment, our estimated metric behaves as expected even at the crossing-fiber region — the geodesics are not confounded in our metric.

3D Brain: To validate our method’s ability to estimate 3D crossing-fiber regions in real brain DWMRI, we used HCP subject 103818. We first reconstructed the vector fields through the GQI method in *DSI Studio* with a diffusion sampling length ratio of 1.25. We then estimated a whole-brain metric by a CEDNN featuring 55, 30, 55 dense layers in each dense block, where we used a learning rate of 0.0003 for a total of 90000 iterations. The top row in Fig. 4 shows the resulting connectome visualized by *3D Slicer* via the *SlicerDMRI* project [25,18]. We show the approximation ability of our method in real-world crossing-fiber region in the bottom of Fig. 4.

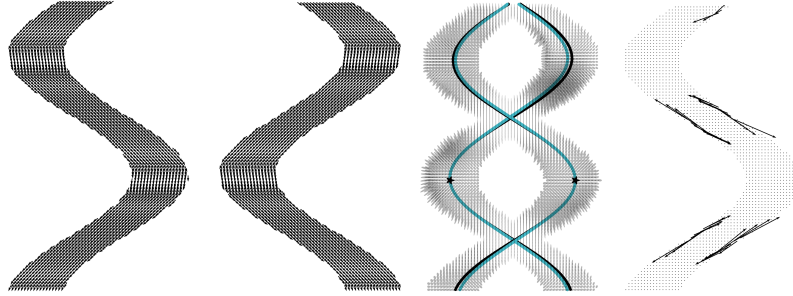


Fig. 3: From left to right: input vector fields \mathbf{v}_1 ; input vector fields \mathbf{v}_2 ; integral curves (black, running on input vector fields) and geodesics (indigo) on estimated Riemannian metric field g at iteration 5000 (background ellipses represent metric tensors), starting from seed points (star); $\nabla_{\mathbf{v}_1}^g \mathbf{v}_1$ visualization at iteration 5000.

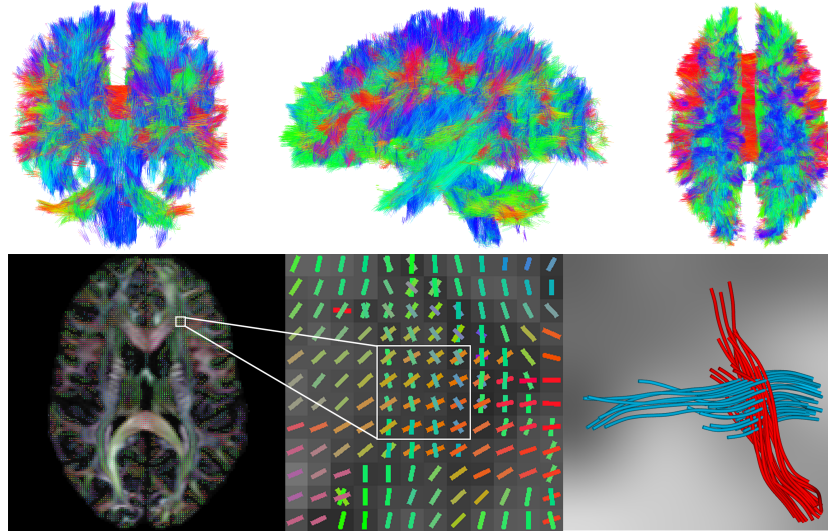


Fig. 4: Top row from left to right: coronal, sagittal, and transversal view of the connectome generated by the proposed method, based on HCP subject 103818. Bottom left: transversal view of the same subject. Bottom central: zoom-in view of a $4 \times 4 \times 4$ crossing-fiber region. Bottom right: geodesic tractography by proposed method starting at $(89, 52, 68)$ within the same window.

5 Conclusion and Future Work

In this paper, we have shown for the first time how we can leverage the flexibility of deep learning to model the shape of the human connectome by estimating a Riemannian metric of the brain manifold. We have not yet studied the generalizability of the network, i.e., it is our aim to further develop the paradigm to train a single network that will efficiently output a metric structure directly from DWMRI data. With the ability to robustly and efficiently model the white matter of the brain as a Riemannian manifold, one can directly apply geometrical statistical techniques such as statistical atlas construction [3], principal geodesic analysis [7], and longitudinal regression [6] to precisely study the variability and differences in white matter architecture.

References

1. Basser, P.J., Pajevic, S., Pierpaoli, C., Duda, J., Aldroubi, A.: In vivo fiber tractography using dt-mri data. *Magnetic resonance in medicine* **44**(4), 625–632 (2000)
2. Behrens, T.E., Woolrich, M.W., Jenkinson, M., Johansen-Berg, H., Nunes, R.G., Clare, S., Matthews, P.M., Brady, J.M., Smith, S.M.: Characterization and propagation of uncertainty in diffusion-weighted mr imaging. *Magnetic Resonance in Medicine: An Official Journal of the International Society for Magnetic Resonance in Medicine* **50**(5), 1077–1088 (2003)
3. Campbell, K.M., Dai, H., Su, Z., Bauer, M., Fletcher, P.T., Joshi, S.C.: Structural connectome atlas construction in the space of Riemannian metrics. In: Feragen, A., Sommer, S., Schnabel, J., Nielsen, M. (eds.) *Information Processing in Medical Imaging*. pp. 291–303. Springer International Publishing (2021)
4. Cheng, G., Salehian, H., Forder, J.R., Vemuri, B.C.: Tractography from hardi using an intrinsic unscented kalman filter. *IEEE transactions on medical imaging* **34**(1), 298–305 (2014)
5. Do Carmo, M.P., Flaherty Francis, J.: *Riemannian geometry*, vol. 6. Springer (1992)
6. Durrleman, S., Pennec, X., Trounev, A., Braga, J., Gerig, G., Ayache, N.: Toward a comprehensive framework for the spatiotemporal statistical analysis of longitudinal shape data. *International journal of computer vision* **103**(1), 22–59 (2013)
7. Fletcher, P.T., Lu, C., Pizer, S.M., Joshi, S.: Principal geodesic analysis for the study of nonlinear statistics of shape. *IEEE transactions on medical imaging* **23**(8), 995–1005 (2004)
8. Fletcher, P.T., Tao, R., Jeong, W.K., Whitaker, R.T.: A volumetric approach to quantifying region-to-region white matter connectivity in diffusion tensor mri. In: *Biennial International Conference on Information Processing in Medical Imaging*. pp. 346–358. Springer (2007)
9. Fuster, A., Haije, T.D., Tristán-Vega, A., Plantinga, B., Westin, C.F., Florack, L.: Adjugate diffusion tensors for geodesic tractography in white matter. *Journal of Mathematical Imaging and Vision* **54**(1), 1–14 (2016)
10. Glasser, M.F., Sotiropoulos, S.N., Wilson, J.A., Coalson, T.S., Fischl, B., Andersson, J.L., Xu, J., Jbabdi, S., Webster, M., Polimeni, J.R., et al.: The minimal preprocessing pipelines for the human connectome project. *Neuroimage* **80**, 105–124 (2013)
11. Gluck, H.: Dynamical behavior of geodesic fields. In: *Global theory of dynamical systems*, pp. 190–215. Springer (1980)
12. Hao, X., Whitaker, R.T., Fletcher, P.T.: Adaptive riemannian metrics for improved geodesic tracking of white matter. In: *Biennial International Conference on Information Processing in Medical Imaging*. pp. 13–24. Springer (2011)
13. He, K., Zhang, X., Ren, S., Sun, J.: Deep residual learning for image recognition. In: *Proceedings of the IEEE conference on computer vision and pattern recognition*. pp. 770–778 (2016)
14. Huang, G., Liu, Z., Van Der Maaten, L., Weinberger, K.Q.: Densely connected convolutional networks. In: *Proceedings of the IEEE conference on computer vision and pattern recognition*. pp. 4700–4708 (2017)
15. Johnson, D.L., Naveira, A.: A topological obstruction to the geodesibility of a foliation of odd dimension. *Geometriae Dedicata* **11**(3), 347–352 (1981)
16. Lee, J.M.: *Introduction to Riemannian manifolds*. Springer (2018)

17. Malcolm, J.G., Shenton, M.E., Rathi, Y.: Neural tractography using an unscented kalman filter. In: International Conference on Information Processing in Medical Imaging. pp. 126–138. Springer (2009)
18. Norton, I., Essayed, W.I., Zhang, F., Pujol, S., Yarmarkovich, A., Golby, A.J., Kindlmann, G., Wassermann, D., Estepar, R.S.J., Rathi, Y., et al.: Slicerdmri: open source diffusion mri software for brain cancer research. *Cancer research* **77**(21), e101–e103 (2017)
19. O’Donnell, L., Haker, S., Westin, C.F.: New approaches to estimation of white matter connectivity in diffusion tensor mri: Elliptic pdes and geodesics in a tensor-warped space. In: International Conference on Medical Image Computing and Computer-Assisted Intervention. pp. 459–466. Springer (2002)
20. Raissi, M., Perdikaris, P., Karniadakis, G.E.: Physics-informed neural networks: A deep learning framework for solving forward and inverse problems involving nonlinear partial differential equations. *Journal of Computational Physics* **378**, 686–707 (2019)
21. Srivastava, R.K., Greff, K., Schmidhuber, J.: Training very deep networks. *Advances in neural information processing systems* **28** (2015)
22. Tuch, D.S.: Q-ball imaging. *Magnetic Resonance in Medicine: An Official Journal of the International Society for Magnetic Resonance in Medicine* **52**(6), 1358–1372 (2004)
23. Tuch, D.S., Reese, T.G., Wiegell, M.R., Makris, N., Belliveau, J.W., Wedeen, V.J.: High angular resolution diffusion imaging reveals intravoxel white matter fiber heterogeneity. *Magnetic Resonance in Medicine: An Official Journal of the International Society for Magnetic Resonance in Medicine* **48**(4), 577–582 (2002)
24. Tuch, D.S., et al.: Diffusion MRI of complex tissue structure. Ph.D. thesis, Massachusetts Institute of Technology (2002)
25. Zhang, F., Noh, T., Juvekar, P., Frisken, S.F., Rigolo, L., Norton, I., Kapur, T., Pujol, S., Wells, W., Yarmarkovich, A., Kindlmann, G., Wassermann, D., San Jose Estepar, R., Rathi, Y., Kikinis, R., Johnson, H.J., Westin, C.F., Pieper, S., Golby, A.J., O’Donnell, L.J.: Slicerdmri: Diffusion mri and tractography research software for brain cancer surgery planning and visualization. *JCO Clinical Cancer Informatics* (4), 299–309 (2020). <https://doi.org/10.1200/CCI.19.00141>, <https://doi.org/10.1200/CCI.19.00141>, PMID: 32216636
26. Zhu, Y., Zabararas, N., Koutsourelakis, P.S., Perdikaris, P.: Physics-constrained deep learning for high-dimensional surrogate modeling and uncertainty quantification without labeled data. *Journal of Computational Physics* **394**, 56–81 (2019)